International Journal of Biological Macromolecules 97 (2017) 23–33

Contents lists available at ScienceDirect

International Journal of Biological Macromolecules

journal homepage: www.elsevier.com/locate/ijbiomac

Enhanced wound healing activity of desert locust *(Schistocerca gregaria)* vs. shrimp *(Penaeus monodon)* chitosan based scaffolds

Narguess H. Marei [a], W. El-Mazny [b], Aida El-Shaer [b], Kareem Dorri Zaki [c], Zahra S. Hussein [d], Emtithal M. Abd-El-Samie [e,*]

[a] *Nanotechnology Program, School of Sciences and Engineering, American University in Cairo, New Cairo, Egypt*
[b] *Research and Development Unit, Holding Company for Biological products and Vaccines-VACSERA, Giza, Egypt*
[c] *Biotechnology Program, Faculty of Sciences, Cairo University, Giza, Egypt*
[d] *Faculty of Biotechnology, Modern Sciences and Arts University, 6th of October, Egypt*
[e] *Entomology Department, Faculty of Sciences, Cairo University, Giza, Egypt*

ARTICLE INFO

Article history:
Received 31 July 2016
Received in revised form
26 December 2016
Accepted 2 January 2017
Available online 3 January 2017

Keywords:
Chitosan
Wound healing
Tissue engineering

ABSTRACT

Chitosan (CS) has received great attention in tissue engineering, especially in wound healing acceleration. In this study, chitin was isolated from desert locust (*Schistocerca gregaria*) and shrimp *(Penaeus monodon)* then deacetylated to chitosan. Then, chitosan was characterized by degree of deacetylation (DD), molecular weight (M.Wt), swelling index (SI), Fourier transform infrared (FTIR) and X ray diffraction (XRD). The chitosan was then casted into 2D scaffolds and was pictured using scanning electron microscope (SEM). In a comparative study, primary cell cultures of neonatal (1–2 day old) mice skin tissue, supplemented with 10% fetal calf serum, were seeded onto locust chitosan based scaffolds (LCSBS) and shrimp chitosan based scaffold (SCSBS). Their attachment percentage was determined after 1 h. The cell proliferation rate was tested for 5 days on LCSBS and SCSBS. Wound healing activity progress of LCSBS and SCSBS was tested in vivo using histopathology, and results revealed that seeded and unseeded LCSBS accelerated healing in contrast to SCSBS. The data demonstrated that LCSBS shows a high degree of biocompatibility in vivo. These results suggest that LCSBS is a potential substitute for the development of low cost implantable materials to accelerate wound healing.

1. Introduction

Biomedical engineering as an interdisciplinary field, aims to regenerate new biological materials using tissue engineering to replace damaged or diseased tissues and organs. Not only is the source of the cells required to achieve this goal, but there is also a need for an artificial extracellular matrix (ECM) that supports cells growth. In humans, skin represents approximately one-tenth of the human body's mass. Skin damage to a part of this major organ caused by disease, trauma, surgery or burns has dramatic consequences. Engineering skin substitutes provides a prospective source of advanced therapy to combat acute and chronic skin wounds [1]. The wound healing process includes hemostasis, inflammation, proliferation, and remodeling [2]. For a wound to heal successfully, it needs an appropriate treatment to modulate a series of complex interactions between different cell types, the ECM and cytokine mediators, through all phases of healing. At the present time, there are no bioengineered skin models that completely mimic the physiology, anatomy and biological stability of uninjured skin [1]. To evaluate various wound medications and dressings, a full thickness skin wound model has been commonly utilized [3–7]. Skin substitutes must have essential characteristics, including: easy application to the wound site, readily adherent, sterile, non-toxic, non-antigenic, antimicrobial with controlled degradation, and processes appropriate physical and mechanical properties. In addition, they should incorporate into the host with minimal pain and scarring, while still being cost effective [1]. The healing of a cutaneous wound includes re-epithelialization, granulation tissue proliferation and collagen synthesis.

There are numerous biomaterials available for wound dressing, including those composed of alginates, polyurethane, hydrocolloids, collagen, pectin, hyaluronic acid and chitosan. The latter is the deacetylated form of chitin, and has been the subject of this study [4,7–12]. Chitin, an ideally 1–4 linked polysaccharide composed of 2 acetamido-2-deoxy-β-D glucopyranosyl residues, is considered the second most abundant biopolymer in nature

* Corresponding author.
E-mail address: emtithal_a@yahoo.com (E.M. Abd-El-Samie).

http://dx.doi.org/10.1016/j.ijbiomac.2017.01.009
0141-8130/

after cellulose. Chitin is available in the exoskeleton of crustaceans, insects, and some fungi species, but rarely exists in a pure form in nature [13]. Insects' biomass is considered to be the alternative resource for chitin, as insects represent the largest resource for chitin as a raw material. Accordingly, the studies of applications of insects' chitin must be taken into consideration [13]. The cuticle of insects is composed of chitin in a matrix with cuticular lipids and proteins [14]. In contrast, the cuticle of crustaceans such as crabs, shrimp, and crayfish is usually composed of chitin in a matrix with protein and minerals [15,16]. Chitosan is composed of (1–4) β linked glucose amine and *N*-acetyl glucosamine units, and its properties depend on its molecular weight, degree of deacetylation, which in turn depend on the production process and the source [17]. Chitosan has been used in countless products, such as cosmetics, food additives, and separation materials. Due to its positive charge, chitosan is a common drug delivery vehicle [18,19]. In addition, chitosan had been used to produce biodegradable films, fibers, cell and enzyme immobilization matrices; healing- accelerating sutures and coverings; contact lenses; and artificial skins [19,20]. Chitosan's biological properties, particularly its nontoxicity, biodegradability, anti-microbial activity, and biocompatibility, resulted in smoother scars and faster healing process. Therefore chitosan became a widely studied skin substitutes [21,22]. One of its most flexible traits is the ability to be fabricated into different forms of scaffold for cell seeding or induction [20]. The aim of this study is to exhibit improved wound healing using locust *(Schistocerca gregaria)* chitosan based scaffolds (LCSBS) and shrimp *(Penaeus monodon)* chitosan based scaffolds (SCSBS) and to compare between insects and crustaceans chitosan powders' physicochemical properties. The study compares between the biocompatibility of the two forms of chitosan in vitro by seeding primary skin cells onto LCSBS and SCSBS and tests the cells' attachment percent and proliferation rate. The mice model was used to test wound closure rates for 21 days using histopathological assessment.

2. Material and methods

2.1. Isolation of chitin and deacetylation to chitosan

Chitosan was extracted from the exoskeleton of giant tiger prawn shrimp (*Penaeus mondon*), collected from Suez gulf, Egypt, and from desert locust (*Schistocerca gregaria)* exoskeletons reared in the Entomology Department, Faculty of Sciences, Cairo University. Chitosan was prepared using the same method and under the same conditions as previously reported [13,23,24]. Briefly, Locusts and shrimp shells were washed and dried then soaked in 1M NaOH as a deproteinization step, followed by the demineralization step using 1N HCl to obtain chitin. Finally the obtained chitin was deacetylated to chitosan using 50% NaOH.

2.2. Physicochemical characterization of chitosan

Fourier transform infrared (FTIR) spectroscopy of locust chitosan (LCS) and shrimp chitosan (SCS) were recorded with the Nicolet iS^{TM}10 FTIR Spectrometer, Thermo Fisher Scientific, USA. Specimens were placed on the KBr diamond. The spectral region between 4000 and 400 cm-1 was scanned with a resolution of 2 cm^{-1} within 20 scans. X-ray diffraction was performed using PANalyticalX'Pert PRO X-ray machine (Netherland). The surface morphology of the dried isolated LCS and SCS was investigated using a field emission scanning electron microscope, FESEM (Leo Supra 55–Zeiss Inc., Germany). The surface images were captured at an accelerating voltage of 15.0 kV at different magnifications.

2.3. Degree of deacetylation determination

Degree of Deacetylation of LCS and SCS was measured using a titration method according to the method of Abdo, Nagy et al. [25]. Briefly 0.5 gm LCS and SCS were weighed and dissolved separately by 0.3N HCL and titrated against 1N NaOH solution (Sigma-Aldrich, US). A titration curve of pH vs. NaOH titration volume was generated. The curve's inflection points were found for each indicated transition. The volume of NaOH at each inflection point was applied to the equation:

$$\%NH2 = \frac{16.1(y - x)}{M}$$

Where M is the weight of chitosan used (0.5 gm), x is the first inflection point on the graph of measured pH vs. titration volume, and y is the second inflection point.

2.4. Elasticity and viscosity average molecular weight determination

The elasticity and viscosity of LCS and SCS were measured by the Piezo Axial Vibrator viscometer. The viscosity average Mwt. was calculated from the intrinsic viscosity [η] using the Mark-Houwink equation

$$[\eta] = K M_v{}^{\alpha}$$

Where, [η] is the intrinsic viscosity, M_v the viscosity-average molecular weight, *K* and a in the equation have been determined in the literature and were adjusted by the degree of deacetylation (DD) according to the following equation:

$K = 1.64 \times 10^{-30} \times DD^{14}$, and $\alpha = -1.02 \times 10{-}2 \times DD + 1.82$ where DD is expressed as the percentage, suitable for the determination of chitosan with over 60% DD [26].

2.5. Preparation and casting of chitosan scaffold

The scaffolds were prepared by dissolving 1gm of LCS and SCS in 1% acetic acid (Sigma-Aldrich, US).The mixtures were then filtered and poured in a flat container then incubated at 50 °C overnight. LCS and SCS dried scaffolds were cut into 1 cm diameter circles then sterilized with gradient concentrations of 95%, 85% and 75% ethanol (Sigma-Aldrich, US), respectively for 20 min [27]. The scaffolds surface morphology was examined using a field emission scanning electron microscope, FESEM (Leo Supra 55–Zeiss Inc., Germany). The surface images were captured at an accelerating voltage of 15.0 KV at different magnifications.

2.6. Swelling index measurement

A dried locust chitosan based scaffold (LCSBS) and shrimp chitosan based scaffold (SCSBS) scaffolds were weighed and immersed in phosphate buffered solution of pH 7.4 for 24 h at room temperature till reaching the swelling equilibrium. The swollen scaffolds weight was determined and their swelling index (SI) was calculated by the following equation:

$$SI = \frac{(Ws - Wd)}{Wd \times 100}$$

Where, W_s and W_d are the weights of swollen and dry samples, respectively [28].

2.7. In vitro biocompatibility study

Primary skin fibroblast cells of neonatal mice origin were used to evaluate the LCSBS and SCSBS on cells adherence and proliferation rate. The preparation of the primary cell culture was done as

previously reported [27,29]. Cytotoxicity was evaluated via seeding the cells onto the LCSBS and SCSBS in a 24 well plate at a density of 5×10^4 cells/well and incubated in a humidified incubator with 5% CO_2 for 24 h at 37 °C [30]. Subsequently, each scaffold was seeded with the cells and incubated for 5 days into CO_2 incubator with 5% CO_2 at 37 °C to allow for cell attachment and proliferation. Triplicate wells were prepared for each sample. After 48 h, the difference in morphology between control cells and those seeded onto scaffolds was observed under the inverted microscope. Cell viability was assessed after day 1 and day 5 via MTT (3-(4, 5-dimethylthiazol-2-yl)-2, 5-diphenyltetrazolium bromide) assay as previously reported [31]. The absorbance was determined at 570 nm and percent of cell survival was calculated according to the following equation:

$$\%\text{Viability} = \frac{(\text{Sample Absorbance} - \text{Blank Absorbance})}{(\text{Negative control Absorbance} - \text{Blank Absorbance})}$$

2.8. In vivo assessment

2.8.1. Mice wound healing model

Animal experiments were performed according to institutional ethical guidelines. Wound healing animal model study was approved from the animal research committee in the Zoology Department, Faculty of Science, Cairo University. In vivo, wound healing was performed on male Balb/c mice of 24 gm weight to evaluate the wound healing ability of LCSBS and SCSBS on the regeneration of the injured skin. All animals were anesthetized with a mixture of ketamine HCl (50 mg/kg) and Xylene HCl (20 mg/Kg). Their backs were then shaved using a depletory cream. A 9 mm wound was created on the back of mice using a biopsy puncher to perform a full thickness wound along the dorsal side of mice skin. Five groups of mice were tested for the change in the healing of the induced injury. The groups were as follow: group 1 (G1) was the control untreated and the injury was covered by cotton gauze, group 2 (G2) was the SCSBS treated wound, group 3 (G3) was the LCSBS treated wound, group 4 (G4) was the SCSBS seeded with 1×10^4 fibroblast cells (FC) and group 5 (G5) was the LCSBS seeded with 1×10^4 FC. Each sample of each group as well as the control group was tested on three mice and the mean value was recorded [9].

2.8.2. Histopathology assessment

At each time point, three mice were euthanized in each group. The wound site with the surrounding muscle and skin was cut and then fixed with 10% buffered formalin. The collected samples were then put in paraffin and sectioned. Each of the tissue samples was then subjected to hematoxylin and eosin (H&E) staining. The stained sections were evaluated and scored at days 1, 3, 5, 14, and 21. The stained sections were evaluated for the following histologic outcomes: necrosis, inflammation, angiogenesis, epithelization, fibroplasia and healing type for neutrophils, macrophages, endothelium, fibrocytes and epidermal cells. A histologic scoring system was used to assess each parameter, and a score of 0–4 was assigned for each sample. Necrosis, inflammation, angiogenesis, epithelization, fibroplasia and healing type were assigned as follow: 0 (absent), 1 (minimal), 2 (mild), 3 (moderate) and 4 (marked) [32]. Since the results are semi-quantitative, the mode value was obtained for each group and statistical comparison intra and inter-groups) was performed to test the significant statistical difference, with $P \leq 0.05$. Moreover, the positive and negative events were also defined according to standard histologic parameters for wound healing. These were quantitated in each group and expressed as:

$$\text{Frequency No} = \frac{\text{No of events}}{\text{Sum of events} \times 100}$$

Table 1
Physicochemical characterization of LCS, SCS, LCSBS and SCSBS.

	LCS	SCS
Degree of deacetylation	97.80%	74%
Molecular weight	1.950 KDa	6.068 KDa
Viscosity	6.15 P	2.57 P
	LCSBS	SCSBS
Elasticity	0.15	−0.15
Swelling Index	13%	88%

3. Results and discussion

3.1. Chitosan extraction and characterization

In recent years, chitosan from unconventional sources such as insect and fungal mycelia has gained more prominence [23,33–35]. Different researchers have reported that chitin and chitosan yields vary between species and seasons of harvest [36]. During this study, the all-round effects of chitosan scaffold from crustacean and insect sources were examined and compared. The exoskeleton percentage to the total body's fresh weight of desert locust (*Schistocerca gregaria*) and shrimp (*Penaeus mondon)* shells' were 26.6% and 39%, respectively. The chitin yield obtained from desert locust was 22.5% and the chitosan yield 55%. The shrimp shells' dry weight was 40%, while chitosan yield 81%. These results are in agreement with the results obtained by the work of Zhang, Haga et al., who reported that silkworms presented an average of 20% of chitin within its structure [33]. The degree of deacetylation, molecular weight and viscosity of LCS and SCS are shown in Table 1. The LCSBS and SCSBS swelling index and elasticity differences are also shown in Table 1. A high swelling degree would cause a decrease in elasticity and thus less strength of chitosan conduits, which can lead to the collapse of the hollow structure [37]. The locust films showed less SI, which could be due to the influence of untested parameters, such as the nature of polymer, polymer chain flexibility, molecular mass, crystal structure, and chemical composition [38]. Proportionally, if there is an increase in DD, the amino groups seem to increase the swelling index of chitosan films but the higher intermolecular bonds prevent water from entering the crystal regions of the material. Finally, the films prepared from higher DD chitosan showed a lower swelling property, which is a good indication that higher DD chitosan conduits are appropriate for clinical applications [39]. The molecular weight (M,Wt) of chitosan has significant impacts on its effectiveness for a variety of applications. This appears in the efficacy of chitosan to accelerate burnt skin healing, coagulate pollutants, lower blood cholesterol levels, enhance drug dissolution, control viscosity which were found to be molecular weight dependent [40]. This relation has been confirmed in this study, where the viscosity of LCS was higher than SCS 6.15 and 2.57 P, respectively, while the molecular weight was 1.950 KDa and 6.068 KDa in LCS and SCS, respectively. The LCS (Fig. 1(A)) and SCS (Fig. 1(B)) surface morphology was examined using the scanning electron microscope showing the fibrous surface structure with a higher surface area. This was the case also when examining the LCSBS (Fig. 1(C)). However, the SCSBS (Fig. 1(D)) showed a smooth surface which is not beneficial in terms of increasing surface area to allow more cells to attach between the fibrous grooves as in the case of LCSBS. FTIR analysis showed in Fig. 2(A). As seen, the absorption peak of amide I (due to —C=O stretching of hydrogen bonded —C=O—$NHCH_3$ group) appears as a doublet overlapped bands at around 1663 and 1618 cm^{-1}, indicating that the isolated chitosans from the tested species are in α form. The amide II (due to N—H bending of —NH_2 group) bands appear at round 1589 cm^{-1} [41–46]. For the SCS, these peaks appeared at 1650 and 1586 cm^{-1}, respectively. The absorption band at 3000–3500 cm^{-1} is due to symmetric stretching vibration of NH_2 and OH groups. The absorption peak at around

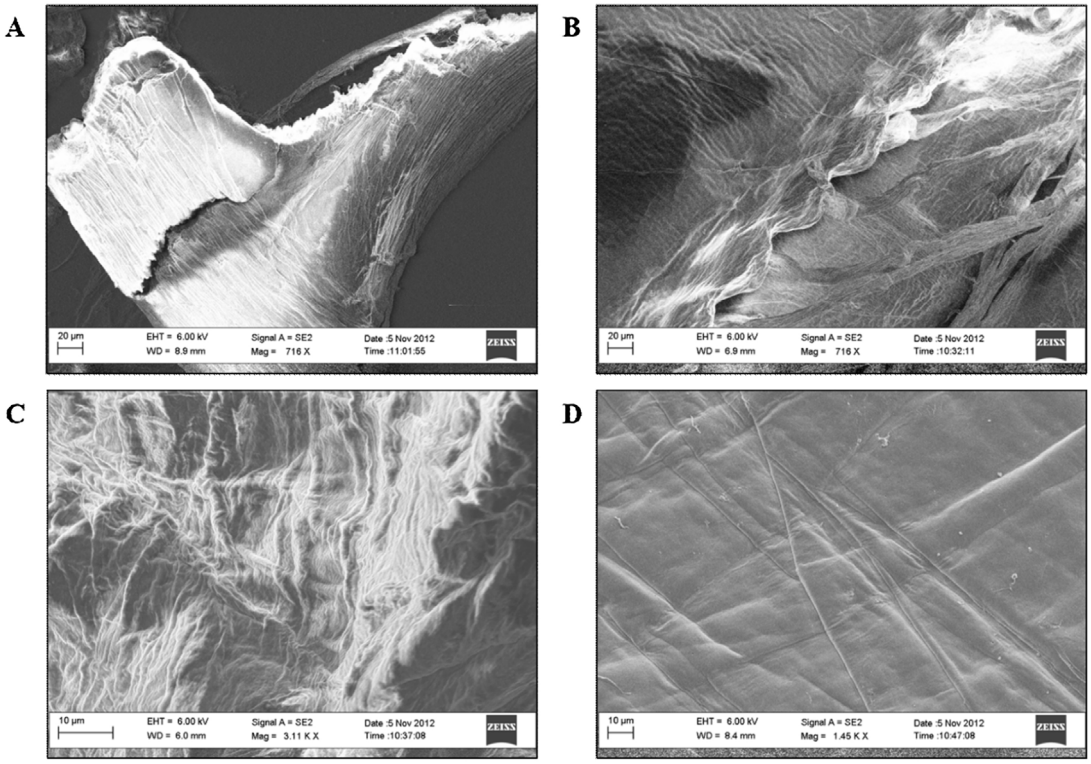

Fig. 1. Scanning electron microscopy imaging of (A) LCS (20 μm), (B) SCS (20 μm), (C) LCSBS (10 μm) and (D) SCSBS (10 μm).

2885 cm^{-1} is due to C—H stretching. The absorption peaks at 1326 and 1080 cm^{-1} are due to N—H bending vibration of primary amides and C—O—C stretching, respectively [47,48]. XRD patterns of LCS and SCS were shown in Fig. 2(B). As seen, SCS exhibited two sharp (9.4° and 20.2°) and two faint (22.0° and 26.8°) diffraction peaks. For LCS, three sharp peaks at 9.3°, 20.2° and 24.4° were observed. Similar peaks were observed in chitin and chitosan structures obtained from different organisms such as insects, crustaceans, anthozoans and fungi [23,49–54]. The two sharp peaks appeared at around 10° and 20° that corresponding to the (0 2 0) and (1 1 0) planes of the crystalline lattice were classically characterizing chitosan [55,56].

3.2. In vitro biocompatibility study

Cells grown with the LCSBS and SCSBS showed similar morphologies to that of the control (data not shown). Primary skin fibroblast cells were seeded onto LCSBS and SCSBS showing high rate of settling and attachment on their surfaces from the first day, but were counted using hemocytometer the attachment rate was higher on LCSBS than SCSBS, 47.6% and 43%, respectively when the cells (Fig. 3(A–C)). On day 5, fibroblast cells attachment percentage seeded onto LCSBS and SCSBS surfaces was 91.5% and 62.4%, respectively (Fig. 3(A, D and E)). The increasing number of adhering cells to air dried chitosan compared to those adhering to the dish surface confirmed by previous studies [57,58]. Ranucci and Ponsonnet showed the higher efficiency of particle cultivation technique compared to cell culture on a flat substrate, such as culture dishes by showing that when the surface is randomly modified, submicron scale roughness significantly affects cell adhesion [59,60]. It also agrees with the results of Deutsch et al. who revealed that the number of neonatal rat primary cardiac myocytes adhered to micro-pegged membranes increased 4-fold in comparison with untextured membranes [61]. Cells proliferation rate was tested on day 1 and day 5 using MTT assay and the results were calculated as percent proliferation (Fig. 3(F)). On day 1 proliferation percent was 1.6% and 1.2% in LCSBS and SCSBS, respectively, while on day 5 proliferation percent was 90.9%, and 68.12% on the surface of LCSBS and SCSBS, respectively (Fig. 3(F)). The difference in cell adhesion to chitosan can be affected in vitro by the degree of deacetylation (DD). The higher the DD of chitosan the higher amount of free amino group on the surface of chitosan producing a positively charged surface which allows the interaction points between the negatively charged cells and the culture surface [62].

3.3. In vivo characterization

The neutrophils have a granular cytoplasm with a segmented horse-shoe eccentric nuclei (Fig. 4(A)). Macrophages are similar to neutrophils, but their nuclei is bilobated (kidney shaped) and they were normally present early during wound healing (Fig. 4(B)). Epithelium cells are arranged in cohesive groups and rested on a basement membrane in order to form the surface lining epithelium. An early epithelization accompanied normal wound healing whereas, delayed or absent epithelization, encountered in pathologic wound healing such as infected or diabetic patient wound (Fig. 4(C)). Fibroblasts are spindle cells with tapering ends that were arranged in bundles within a collagenous matrix. Early stages of wound healing were characterized by immature fibrous proliferation (granulation tissue), formed mostly of fibroblasts with minimal collagenous matrix (Fig. 4(D)). The endothelial cells are polygonal ovoid cells with abundant cytoplasm and possess rounded margin. Their nuclei is centrally located and ovoid, elongated with blunt ends (cigar shaped). At early stages of wound healing, immature vascular proliferation is encountered, which is characterized by irregular lumina, lacking thick outer muscular layer (Fig. 4(E) left). At later stages, endothelium starts to maturate, with circular arrangement, forming regular vascular space with luminal red blood cells (RBCs) and outer thick circumferential smooth muscle wall (Fig. 4(E) right) [63]. In our study mice wounded tissues were examined using hematoxylin and eosin (H&E) and histopatholog-

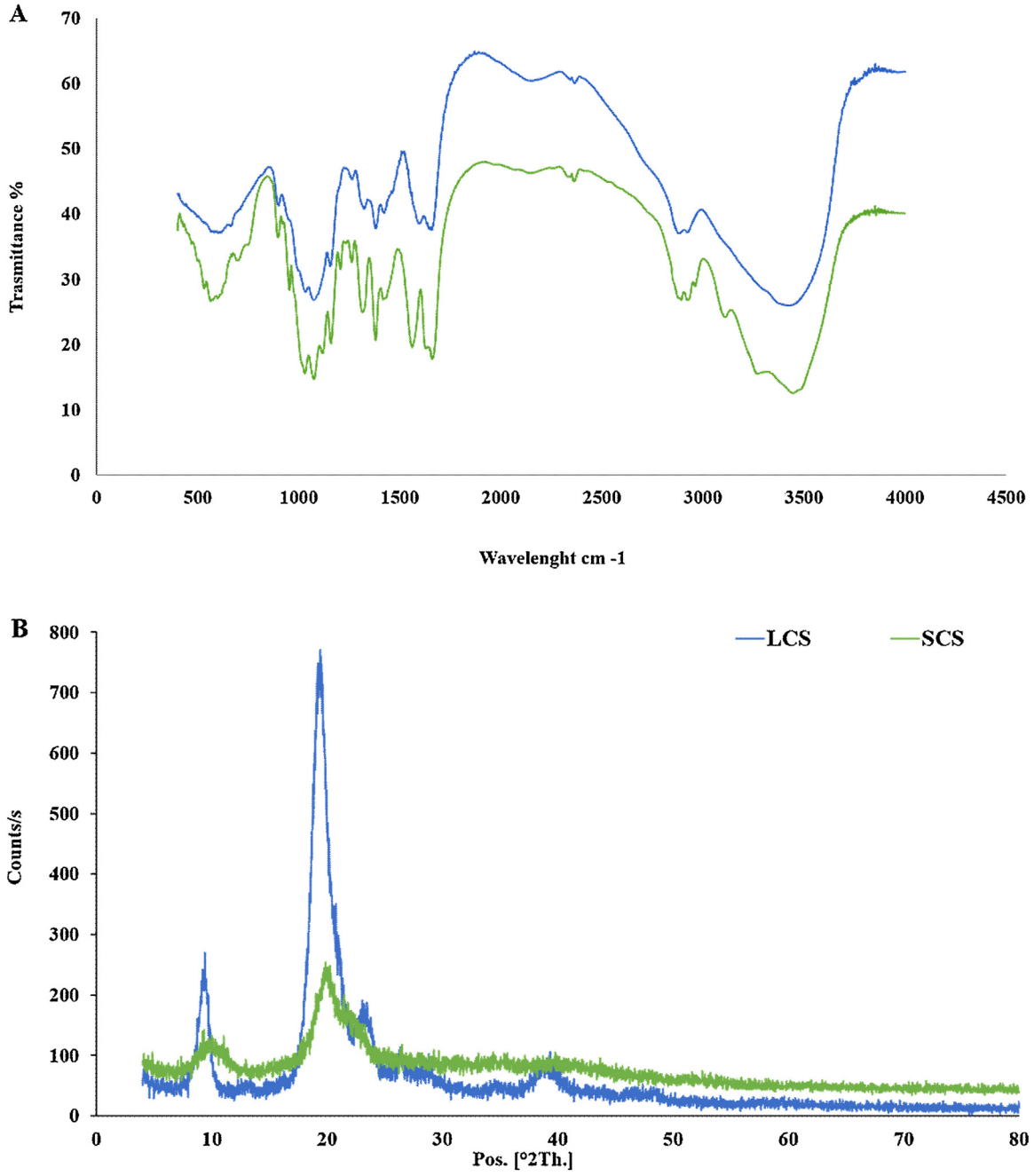

Fig. 2. (A) FTIR, (B) XRD for LCS and SCS.

icaly scored on days 1, 3, 5, 14 and 21 to investigate both locust based chitosan scaffold (LCSBS) and shrimp based chitosan scaffold (SCSBS) wound healing effect as compared to the normal wound closure. Granulation tissues, inflammatory fluid exudates, inflammatory cells, necrosis, epithelization, angiogenesis and thick epidermis formulation were the parameters used to investigate the quality of the wound healing process quantitatively in vivo. The microscopic histopathological findings indicated that all of the developed unseeded and seeded LCSBS and SCSBS with primary skin cells when applied to the wound site reduced the necrosis as compared to the control in which the inflammatory necrotic cells were observed at a higher level after 5 days and continued until day 14 this was due to the continuity of necrosis and sub-epithelial fibroplasia within the wound tissue. Moreover, minimal epithelization started on day 14 in the wound area of the control which means that the quality of the healing process was very poor (Figs. 5–7). Additionally, it was observed that the number of macrophage cells decreased slightly with increasing implant duration. It was greater in all developed scaffolds including the control on day 3 than seeded locust LCSBS, therefore they completely diminished on day 5 and 14 in seeded LCSBS and seeded SCSBS, respectively (Fig. 8). The results were inconsistent with previously work which explained that, the rats receiving the primary skin stem cells containing chitosan scaffold showed slightly less macrophages than chitosan scaffold only, due to the unique immune modulatory properties of stem cells [64–66]. Glycan was known as a macrophage activating agent and accelerating the cytokine production from macrophage [67,68]. Chitosan is a polysaccharide as well as glycan; therefore chitosan also may produce the cytokine which can promote tissue repair. Also, it was found in previous study on dogs that collagen synthesis

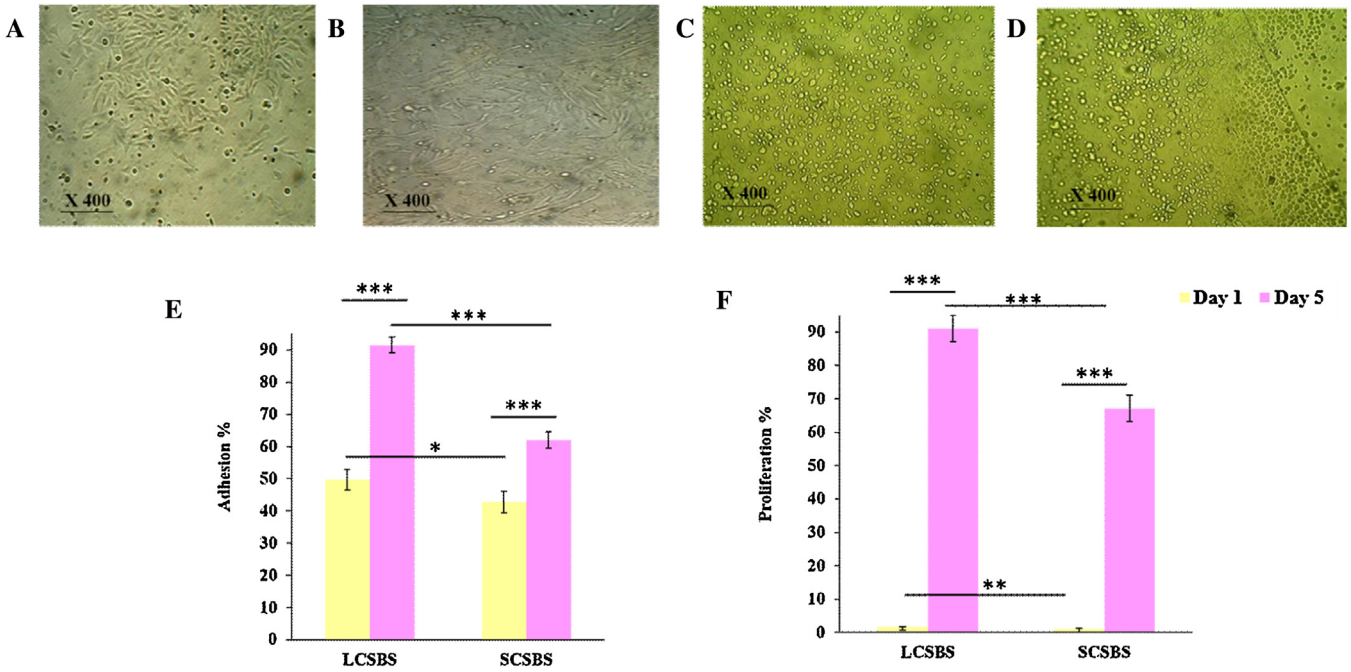

Fig. 3. Day 1 cultured fibroblasts cells seeded onto (A) SCSBS (B) LCSBS. Day 5 cultured fibroblasts cells seeded onto (C) SCSBS (D) LCSBS, (E) percent adhesion and (F) percent proliferation of cultured fibroblasts cells seeded onto SCSBS and LCSBS at day 0 and day 5, respectively. Unpaired T-test was used for performing statistics; *** $P \leq 0.01$, **$P \leq 0.05$, and *$P \leq 0.06$. Error bars indicate SD.

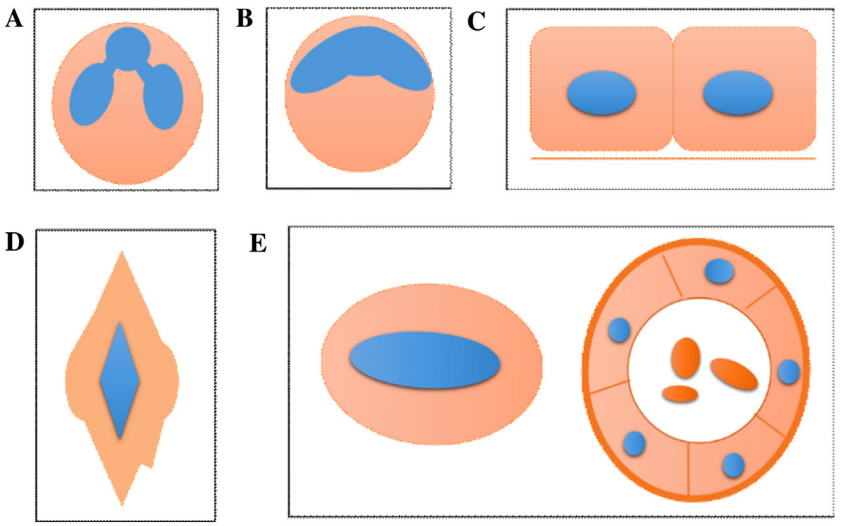

Fig. 4. Graphical representation of (A) neutrophils, (B) macrophages, (C) epithelium, (D) fibroblasts and (E) endothelium.

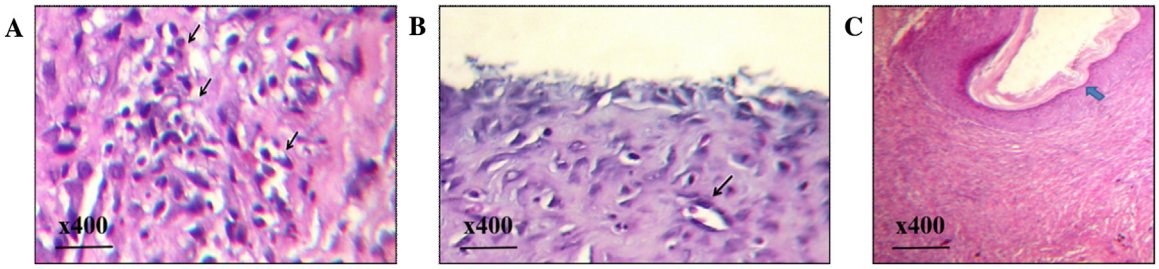

Fig. 5. Histopathological examination for G1 (H&E). (A) day 5: The inflammatory exudates (arrows) are marked (score 3–4), mostly of neutrophils (score 4) with marked necrosis, poor vasculature and immature granulation tissue. (B) Day 14: poor healing is evident in the form of immature sub-epithelial fibroplasia (hypercellular granulation with minimal stromal fibro-collagenosis), as well, as low vasculature of immature blood vessels (arrow). There is minimal epithelization (upper field). (C) Day 21: complete wound closure, showing surface keratin, which differs from scaffolds, being wavy, pale pink and in intimate relation to the upper layer keratinocytes with tendency for micro keratocyst formation. (For interpretation of the references to colour in this figure legend, the reader is referred to the web version of this article.)

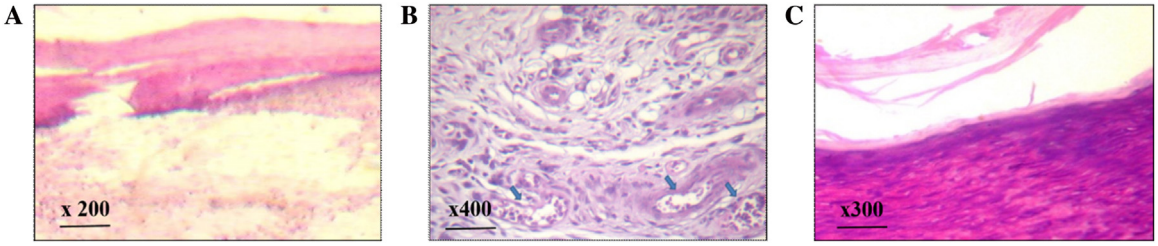

Fig. 6. Histopathological examination for G2 (H&E) (A) Day 1: a minimal inflammation (score 1) is encountered at the lower field with associated tissue edema. The scaffold appears pinkish, laminated and refractile with no attempt for structural degradation nor tissue absorption. (B) Day 14: early wound closure failure with subepithelial proliferating septic and vascular granulation tissue. Blood vessels are immature (arrows), appearing irregular with luminal RBCs. (C) Day 21: wound complete epithelization (arrows). There is dermal fibrosis (score 2), appearing immature with high cell/stroma ration. Inflammation and angiogenesis are minimal. (For interpretation of the references to colour in this figure legend, the reader is referred to the web version of this article.)

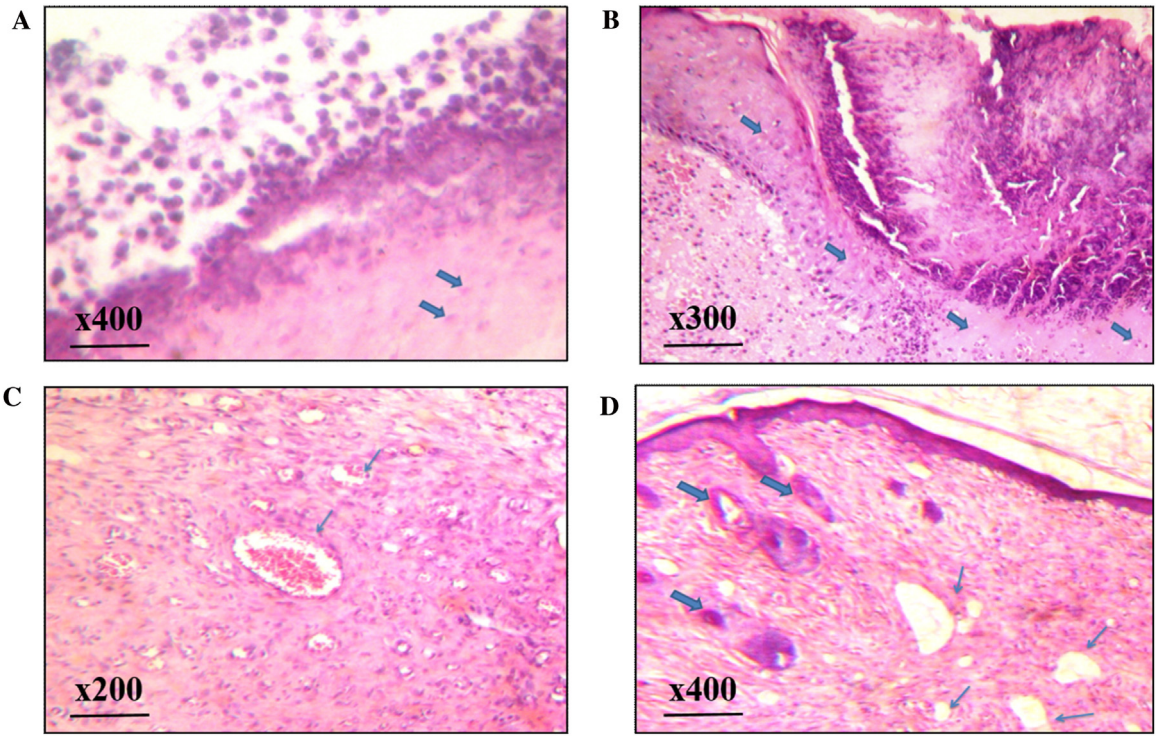

Fig. 7. Histopathological examination for G3 (H&E). (A) Day 1: these are primitive small cells, with no yet evidence of epidermal lineage of differentiation. The lower Rt. Area of the field represents the surface wound with secondary early tissue reaction to injury of proteincious inflammatory fluid exudates appearing pale pinkish and structureless with granular necrotic debris and ghosts of degenerated cells (arrows). (B) Day 5: there is evidence of epidermal differentiation (arrows), showing pinkish cytoplasmic kerato hyaline granules and active attempt for wound closure (epithelization with score 3). The lower Lt. area of the field represents tissue reaction of inflammatory cellular and fluid exudates, as well as, granular necrotic debris of ghosts of degenerated cells. Angiofibroplasia is encountered but both elements were immature. (C) Day 14: there is marked angiofibroplasia, at the subepidermal tissue, yet blood vessels are predominantly immature and some show luminal RBCs (arrows). (D) Day 14: the field represented the edge of the wound with normal skin entangling hair follicles (bold arrows) at the Lt. side, while the Rt area of the field showed dermal fibrous tissue proliferation and upper surface epithelization (score 4), with near total wound closure. Inflammatory activity is minimal (score 1). Dermal angiogenesis was encountered as proliferating irregular thin walled vascular spaces (thin arrows). (For interpretation of the references to colour in this figure legend, the reader is referred to the web version of this article.)

was increased at early phases of wound healing with chitosan treatment [69]. As compared to the control, our results demonstrated that primary skin cells seeded onto LCSBS and SCSBS showed the earliest granulation tissue formation, angiogenesis, epithelization as well as thicker epidermis formation (Figs. 9 and 10). In skin wound healing, growth factors act as stimulators of fibroblast proliferation and synthesis of extra cellular matrix (ECM) proteins. Chitosan has been reported to indirectly enhance cell proliferation in vivo [70]. For this reason, the present study was not only investigated to show the degree of the implantable scaffolds contribution to the new skin formation, but also to determine the effects of seeded scaffold with primary skin cells on the skin regeneration and wound healing as compared to unseeded scaffolds while comparing at the same time the effect of chitosan source (locust and shrimp). This might be due to that chitin-based dressings were depolymerized, and that oligomers are further hydrolyzed to *N*-acetyl glucosamine, a common amino-sugar in the body, which enters the innate metabolic pathway to be incorporated into glycoproteins [71]. In our findings, seeded LCSBS exhibited the most enhanced effect on wound healing followed by seeded SCSBS as compared with the unseeded scaffolds of both LCSBS, SCSBS and the control. Seeded LCSBS showed dermis active angiogenesis, with a significantly higher count than in the other four groups. There was complete wound closure, with marked epithelization on day 14 in seeded LCSBS and SCSBS, while in the unseeded LCSBS and SCSBS incomplete wound closure was observed at the same day as compared with control group in which poor delayed epithelization that ended by secondary intension healing was observed (Fig. 9 and 10). The healing time was 14 days for the seeded LCSBS and SCSBS with complete degradation of chitosan scaffolds and tissue absorption,

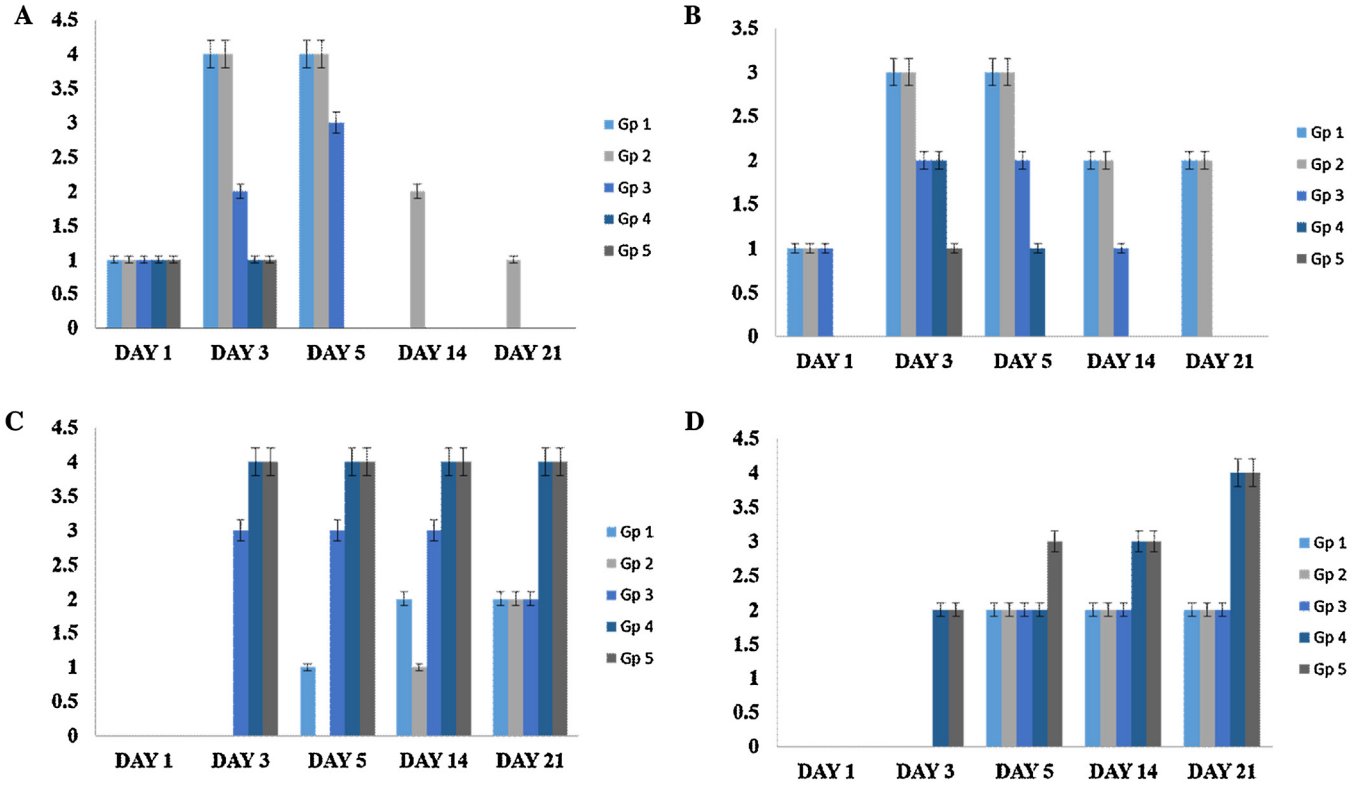

Fig. 8. The distribution of histopathological scores expressed as the mode value among (A) neutrophil, (B) macrophage, (C) endothelium and (D) fibroblast.

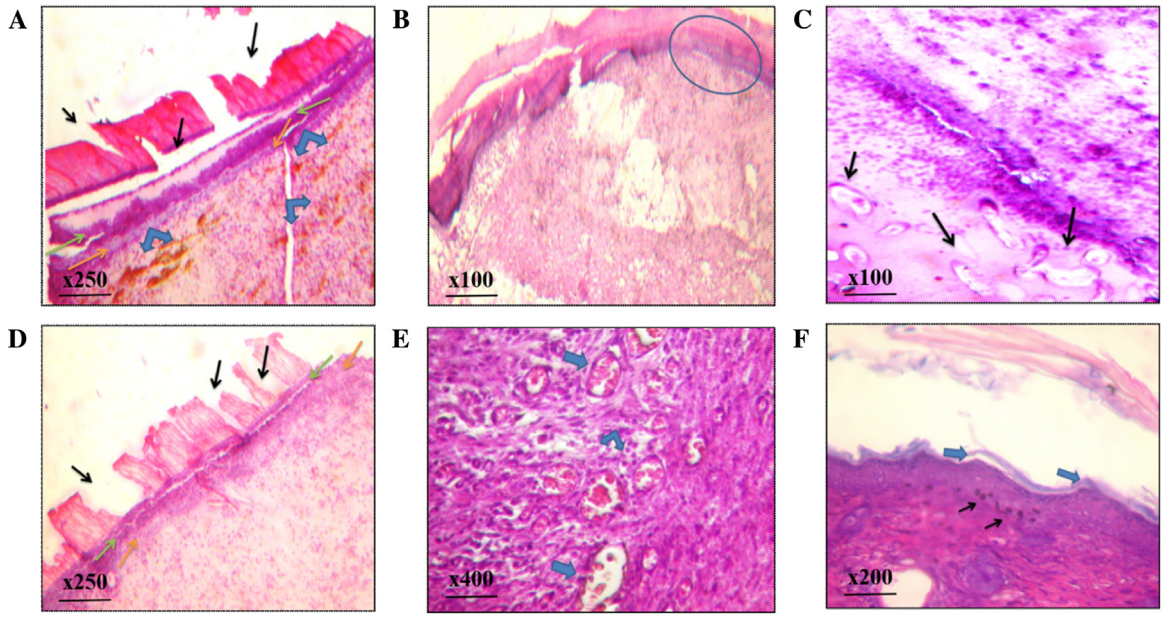

Fig. 9. Histopathological examination for G4 (H&E). (A) Day 3: early tissue reaction to injury of inflammatory cellular exudates, mostly of macrophages (score2). Inflammation is mild and rapidly progressive and associated with proliferating blood vessels of high count (score 4). These show congestion and extravasations of RBCs (blue arrows) with brownish hemosiderin pigmentation. There is an early attempts for epithelization (score 3), appearing as a pale area (orange arrows) below at the interface of the wound surface. It is associated with epidermal differentiation. The layer of stem cells appears dark blue, composed of immature pluripotent cells (green arrows). The scaffold appears dark pinkish retractile with partial degradation (black arrows) with decreased length and thickness as well as focal discontinuity. (Rt.) (B) Day 3: Lt., wound surface early attempts for epithelization (score 3), with partial scaffold degradation. Rt: magnified field of wound surface, showing primitive immature stem cells (upper Rt), undergoing early epidermal differentiation (lower Lt.). (C) Day 3: the mature epidermocytes are rich in cytoplasmic keratohyaline pink granules and exhibit distinct cell borders (arrows). (D) Day 5: regression of inflammation appears (score 1). The layer of epidermal differentiation and epithelization is getting wider with eosinophilic keratosis (evident maturation). (E) Day 5: there is an early increase of angiogenesis (score-4), which is sustained during the healing process, with the predominance of the mature vessels (arrows). (F) Day 14: there is complete wound closure with marked epithelization (score 4). Normal epidermal maturation is evident with surface keratosis (blue arrow), as well as basal melanocytic differentiation, associated with melanin pigmentation (black arrow). The dermis show maturation of fibrous with increased fibro-collagenous matrix and decreased cellularity. The scaffold at upper Rt. field was markedly degraded and the remnants are separated from the healed wound. (For interpretation of the references to colour in this figure legend, the reader is referred to the web version of this article.)

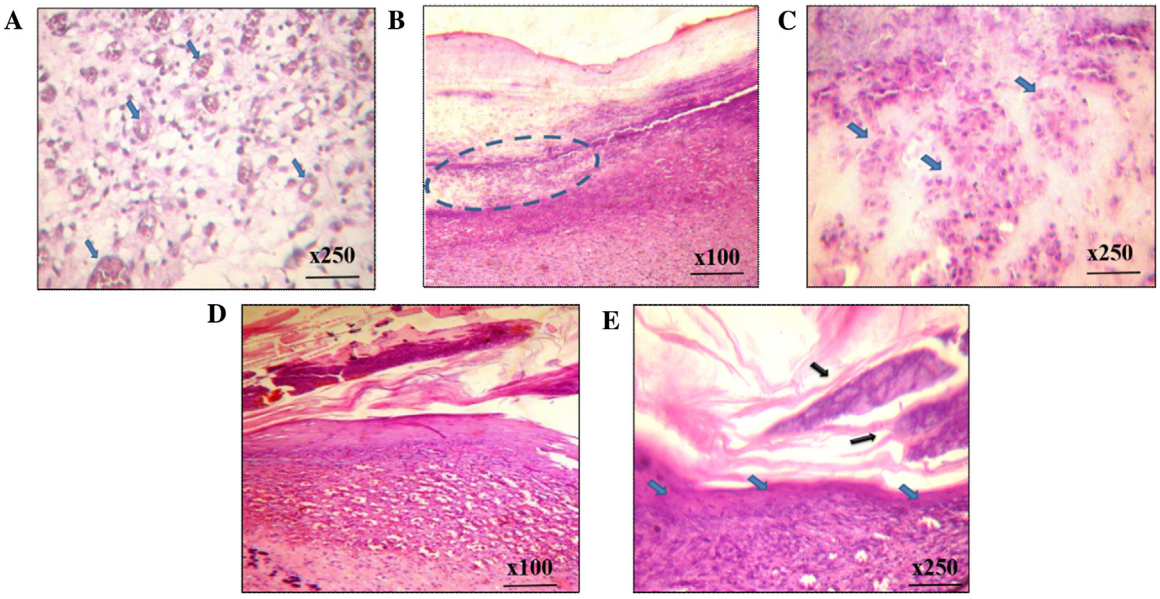

Fig. 10. Histopathological examination for G5 (H&E). (A) Day 3: there was a minimal inflammation (macrophages and neutrophils (score 1)) with marked early angiogenesis (score 4), predominantly of mature thick walled blood vessels (arrows). Fibroplasia was also apparent with early maturation. (B) Day 5: (Lt.) early marked epithelization (score 4) with stem cell maturation (encircled) forming the epidermal layers. Scaffold resorption was encountered and proportionate to the stem cell differentiation and proliferation activity. The subepidermal tissue showed active angiofibroplasia. (C) Day 5: (Rt.) the upper area of the field showed immature stem cells with epithelial differentiation (arrows). The later showed some mature rich in cytoplasmic pinkish hyaline keratogranules. The intervening matrix was rich in keratin. (D) Day 14: (Lt.) early wound closure and epidermal maturation. Scaffold resorption was marked. The dermis active angiogenesis (score 4) with a significantly higher count than the other four groups. (E) Day 14: (Rt.) the stem cells showed active epithelial differentiation (blue arrows) with complete resemblance to the normal epidermal layers. The upper area showed markedly degraded scaffold in proportionate to the degree epithelization. The scaffold entangled few residual islands of residual stem cells (black arrows). (For interpretation of the references to colour in this figure legend, the reader is referred to the web version of this article.)

while it extended to 21 days for the unseeded LCSBS and SCSBS as well as the control (Figs. 5–7). Although, both unseeded LCSBS and SCSBS increased wound healing rates and reduced scar formation when compared with the control. The unseeded SCSBS exhibited the lowest enhanced effect on wound healing among the developed scaffolds. The results of the four groups under study were statistically significant ($P \leq 0.05$) in comparison to the control group. Our results are in agreement with a previous study on the effect of cultural epidermal allografts (CEAL) obtained from young healthy donors, and fixed on tulle grass carrier (Grasolind) in comparison with empty Grasolind. It was reported that the reduction of the non-epithelialized wound area was 86.5% when covered in CEAL, and only 71.2% when covered with Grasolind only and this difference was statistically significant [72]. Also, when studying allograft effect of rat oral mucosa fibroblasts as new seed cells incorporated into collagen and chitosan collagen to construct the tissue engineered oral mucosa lamina, it was found that both the fibroblast populated chitosan collagen lattices can repair skin defects on Wistar rats effectively and feasible [73]. Moreover, the gelatin based scaffolds incorporated with fibroblasts isolated from a child's foreskin enhanced the wound healing rate and re-epithelization of a full thickness skin defect rather than the cellular scaffold after one week [74]. Overall, our histopathological findings indicated that among the tested scaffolds, seeded LCSBS could be the ideal candidate for the development of low cost implantable materials for enhancing wound healing process.

4. Conclusion

In this study chitosan (CS) was isolated from desert locust (*Schistocerca gregaria*) LCS and shrimp (*Penaeus monodon*) SCS and their characteristics were compared physicochemically. Their wound healing activity was also compared when casted as scaffold both in vitro and in vivo. LCS and SCS were characterized using Fourier transform infrared (FTIR) and X ray diffraction (XRD), degree of deacetylation (DD), molecular weight (M.Wt), swelling index (SI) and viscosity. The LCS characteristics were better than shrimp. LCS showed lower SI than shrimp which explained its high elasticity and strength when casted into 2D scaffold that prevented the collapse of the hollow structure. LCS showed a lower M.Wt than SCS which had a significant impact on its effectiveness to accelerate wound healing. This was reflected from its morphological structure when examined using scanning electron microscope (SEM) both LCS powder and the casted LBCS showed a fibrous structure with a high surface to allow more cells to attach between the fibrous grooves compared to SCS powder and the smooth SBCS. This was explained by the in vitro study in which LBCS showed the highest level of cell viability, attachment and proliferation at day 1 and day 5 than SBCS. These results were confirmed by the in vivo study which indicated that among the tested chitosan scaffolds seeded LCSBS performed better than the other groups when examining the wounded tissue using histopathology. It exhibited not only the most enhanced effect on wound healing but also a good healing process quality as well. This was indicated by the scores of the histopathological data of the healed wounds that it showed earlier granulation as well as dermis active angiogenesis with a significantly higher count with early marked epithelization and formation of thicker epidermis with minimal inflammation than in the other groups. Therefore, the wound healing properties of LCSBS makes it low cost competitive material for wound dressing.

References

[1] A.D. Metcalfe, M.W. Ferguson, Tissue engineering of replacement skin: the crossroads of biomaterials, wound healing, embryonic development, stem cells and regeneration, J. R. Soc. Interface 4 (14) (2007) 413–437.
[2] R.F. Diegelmann, M.C. Evans, Wound healing: an overview of acute, fibrotic and delayed healing, Front. Biosci. 9 (1) (2004) 283–289.
[3] I. Strehin, Z. Nahas, M. Rich, G. Marti, X. Zhang, J. Harmon, J. Elisseeff, A bioadhesive and bacteriostatic chondroitin sulfate-polyethylene glycol hydrogel dressing improves survival and rate of wound closure in a mouse

model, wound repair and regeneration, Wound Repair Regen. 19 (2) (2011) A54.
[4] H.-J. Lim, H.-T. Kim, E.-J. Oh, J.-H. Choi, H.-D. Ghim, D.-G. Pyun, S.-B. Lee, D.-J. Chung, H.-Y. Chung, Effect of newly developed pectin/CMC dressing materials on three different types of wound model, Korea Polym. J. 34 (4) (2010) 363–368.
[5] K. Spiess, A. Lammel, T. Scheibel, Recombinant spider silk proteins for applications in biomaterials, Macromol. Biosci. 10 (9) (2010) 998–1007.
[6] G.D. Mogoşanu, A.M. Grumezescu, Natural and synthetic polymers for wounds and burns dressing, Int. J. Pharm. 463 (2) (2014) 127–136.
[7] D. Konrad, M. Tsunoda, K. Weber, S. Corney, L. Ullmann, Effects of a topical silver sulfadiazine polyurethane dressing (Mikacure) on wound healing in experimentally infected wounds in the pig. A pilot study, J. Exp. Anim. Sci. 42 (1) (2002) 31–43.
[8] D. Wyatt, D.N. Mcgowan, M.P. Najarian, Comparison of a hydrocolloid dressing and silver sulfadiazine cream in the outpatient management of second-degree burns, J. Trauma Acute Care Surg. 30 (7) (1990) 857–865.
[9] E.S. Gil, B. Panilaitis, E. Bellas, D.L. Kaplan, Functionalized silk biomaterials for wound healing, Adv. Healthcare Mater. 2 (1) (2013) 206–217.
[10] H.M. Powell, D.M. Supp, S.T. Boyce, Influence of electrospun collagen on wound contraction of engineered skin substitutes, Biomaterials 29 (7) (2008) 834–843.
[11] S.-Y. Ong, J. Wu, S.M. Moochhala, M.-H. Tan, J. Lu, Development of a chitosan-based wound dressing with improved hemostatic and antimicrobial properties, Biomaterials 29 (32) (2008) 4323–4332.
[12] R. Uppal, G.N. Ramaswamy, C. Arnold, R. Goodband, Y. Wang, Hyaluronic acid nanofiber wound dressing—production, characterization, and in vivo behavior, J. Biomed. Mater. Res. B Appl. Biomater. 97 (1) (2011) 20–29.
[13] J. Majtán, K. Bíliková, O. Markovič, J. Gróf, G. Kogan, J. Šimúth, Isolation and characterization of chitin from bumblebee (Bombus terrestris), Int. J. Biol. Macromol. 40 (3) (2007) 237–241.
[14] A. Neville, D. Parry, J. Woodhead-Galloway, The chitin crystallite in arthropod cuticle, J. Cell Sci. 21 (1) (1976) 73–82.
[15] A.T. Showler, Locust (Orthoptera: Acrididae) outbreak in Africa and Asia, 1992–1994: an overview, Am. Entomol. 41 (3) (1995) 179–185.
[16] M. Pener, Y. Yerushalmi, The physiology of locust phase polymorphism: an update, J. Insect Physiol. 44 (5) (1998) 365–377.
[17] M.R. Kumar, R.A. Muzzarelli, C. Muzzarelli, H. Sashiwa, A. Domb, Chitosan chemistry and pharmaceutical perspectives, Chem. Rev. 104 (12) (2004) 6017–6084.
[18] C. Wiegand, D. Winter, U.-C. Hipler, Molecular-weight-dependent toxic effects of chitosans on the human keratinocyte cell line HaCaT, Skin Pharmacol. Physiol. 23 (3) (2010) 164–170.
[19] A.R.C. Duarte, J.F. Mano, R.L. Reis, The role of organic solvent on the preparation of chitosan scaffolds by supercritical assisted phase inversion, J. Supercrit. Fluids 72 (2012) 326–332.
[20] S. Cardea, P. Pisanti, E. Reverchon, Generation of chitosan nanoporous structures for tissue engineering applications using a supercritical fluid assisted process, J. Supercrit. Fluids 54 (3) (2010) 290–295.
[21] Y. Shigemasa, S. Minami, Applications of chitin and chitosan for biomaterials, Biotechnol. Genet. Eng. Rev. 13 (1) (1996) 383–420.
[22] R. Jayakumar, M. Prabaharan, P.S. Kumar, S. Nair, H. Tamura, Biomaterials based on chitin and chitosan in wound dressing applications, Biotechnol. Adv. 29 (3) (2011) 322–337.
[23] N.H. Marei, E.A. El-Samie, T. Salah, G.R. Saad, A.H. Elwahy, Isolation and characterization of chitosan from different local insects in Egypt, Int. J. Biol. Macromol. 82 (2016) 871–877.
[24] F.H. Wilt, C.A. Ettensohn, The morphogenesis and biomineralization of the sea urchin larval skeleton, in: Handbook of Biomineralization: Biological Aspects and Structure Formation, first ed., Wiley Sons, New York, 2007, pp. 182–210.
[25] E.S. Abdou, K.S. Nagy, M.Z. Elsabee, Extraction and characterization of chitin and chitosan from local sources, Bioresour. Technol. 99 (5) (2008) 1359–1367.
[26] H. Xie, S. Zhang, S. Li, Chitin and chitosan dissolved in ionic liquids as reversible sorbents of CO_2, Green Chem. 8 (7) (2006) 630–633.
[27] O. Felt, P. Furrer, J. Mayer, B. Plazonnet, P. Buri, R. Gurny, Topical use of chitosan in ophthalmology: tolerance assessment and evaluation of precorneal retention, Int. J. Pharm. 180 (2) (1999) 185–193.
[28] K.T. Hwang, J.T. Kim, S.T. Jung, G.S. Cho, H.J. Park, Properties of chitosan-based biopolymer films with various degrees of deacetylation and molecular weights, J. Appl. Polym. Sci. 89 (13) (2003) 3476–3484.
[29] A. Seluanov, A. Vaidya, V. Gorbunova, Establishing primary adult fibroblast cultures from rodents, J. Vis. Exp. 44 (2010).
[30] T. Lam, M. Linnes, C. Giachelli, B.D. Ratner, Mechanical testing and optimizing cell seeding on porous fibrin scaffolds, J. Undergrad. Res. Bioeng. 7 (1) (2007) 22–28.
[31] P. Senthilraja, K. Kathiresan, In vitro cytotoxicity MTT assay in Vero, HepG2 and MCF-7 cell lines study of Marine Yeast, J. App. Pharm. Sci. 5 (3) (2015) 80–84.
[32] P. Zahedi, I. Rezaeian, S.H. Jafari, In vitro and in vivo evaluations of phenytoin sodium-loaded electrospun PVA, PCL, and their hybrid nanofibrous mats for use as active wound dressings, J. Mater. Sci. 48 (8) (2013) 3147–3159.
[33] M. Zhang, A. Haga, H. Sekiguchi, S. Hirano, Structure of insect chitin isolated from beetle larva cuticle and silkworm (Bombyx mori) pupa exuvia, Int. J. Biol. Macromol. 27 (1) (2000) 99–105.
[34] W.L. Teng, E. Khor, T.K. Tan, L.Y. Lim, S.C. Tan, Concurrent production of chitin from shrimp shells and fungi, Carbohydr. Res. 332 (3) (2001) 305–316.
[35] S. Nemtsev, O.Y. Zueva, M. Khismatullin, A. Albulov, V. Varlamov, Isolation of chitin and chitosan from honeybees, Appl. Biochem. Microbiol. 40 (1) (2004) 39–43.
[36] E.J. Kramer, P. Green, C.J. Palmstrøm, Interdiffusion and marker movements in concentrated polymer–polymer diffusion couples, Polymer 25 (4) (1984) 473–480.
[37] C. Wenling, J. Duohui, L. Jiamou, G. Yandao, Z. Nanming, Z. Xiufang, Effects of the degree of deacetylation on the physicochemical properties and Schwann cell affinity of chitosan films, J. Biomater. Appl. 20 (2) (2005) 157–177.
[38] S. Taghizadeh, G. Davari, Preparation, characterization, and swelling behavior of *N*-acetylated and deacetylated chitosans, Carbohydr. Polym. 64 (1) (2006) 9–15.
[39] Y. Wan, K.A. Creber, B. Peppley, V.T. Bui, Ionic conductivity of chitosan membranes, Polymer 44 (4) (2003) 1057–1065.
[40] V. Hamilton, Y. Yuan, D.A. Rigney, A.D. Puckett, J.L. Ong, Y. Yang, S.H. Elder, J.D. Bumgardner, Characterization of chitosan films and effects on fibroblast cell attachment and proliferation, J. Mater. Sci.: Mater. Med. 17 (12) (2006) 1373–1381.
[41] M. Kaya, T. Baran, S. Erdoğan, A. Menteş, M. Aşan Özüsağlam, Y.S. Çakmak, Physicochemical comparison of chitin and chitosan obtained from larvae and adult Colorado potato beetle (Leptinotarsa decemlineata), Mater. Sci. Eng.: C. 45 (2014) 72–81.
[42] M. Kaya, N. Bağrıaçık, O. Seyyar, T. Baran, Comparison of chitin structures derived from three common wasp species (Vespa crabro Linnaeus, 1758, Vespa orientalis Linnaeus, 1771 and Vespula germanica (Fabricius, 1793)), Insect Biochem. Physiol. 89 (4) (2015) 204–217.
[43] M. Kaya, M.G. Halıcı, F. Duman, S. Erdoğan, T. Baran, Characterisation of α-chitin extracted from a lichenised fungus species Xanthoria parietina, Nat. Prod. Res. 29 (13) (2015) 1280–1284.
[44] M. Kaya, M. Karaarslan, T. Baran, E. Can, G. Ekemen, B. Bitim, F. Duman, The quick extraction of chitin from an epizoic crustacean species (Chelonibia patula), Nat. Prod. Res. 28 (23) (2014) 2186–2190.
[45] M. Kaya, T. Baran, I. Saman, M.A. Ozusaglam, Y.S. Cakmak, A. Menteş, Physicochemical characterization of chitin and chitosan obtained from resting eggs of Ceriodaphnia quadrangula (Branchiopoda: Cladocera: Daphniidae), J. Crustacean Biol. 34 (2) (2014) 283–288.
[46] M. Kaya, K.Ö. Tozak, T. Baran, G. Sezen, I. Sargin, Natural porous and nano fiber chitin structure from Gammarus argaeus (Gammaridae Crustacea), EXCLI J. 12 (2013) 503–510.
[47] S. Chatterjee, M. Adhya, A. Guha, B. Chatterjee, Chitosan from Mucor rouxii: production and physico-chemical characterization, Process Biochem. 40 (1) (2005) 395–400.
[48] R. Jayakumar, M. Prabaharan, R. Reis, J. Mano, Graft copolymerized chitosan—present status and applications, Carbohydr. Polym. 62 (2) (2005) 142–158.
[49] Y. Wang, Y. Chang, L. Yu, C. Zhang, X. Xu, Y. Xue, Z. Li, C. Xue, Crystalline structure and thermal property characterization of chitin from Antarctic krill (Euphausia superba), Carbohydr. Polym. 92 (1) (2013) 90–97.
[50] M.-T. Yen, J.-H. Yang, J.-L. Mau, Physicochemical characterization of chitin and chitosan from crab shells, Carbohydr. Polym. 75 (1) (2009) 15–21.
[51] W. Sajomsang, P. Gonil, Preparation and characterization of α-chitin from cicada sloughs, Mater. Sci. Eng. C 30 (3) (2010) 357–363.
[52] M. Kaya, T. Baran, M. Asan-Ozusaglam, Y.S. Cakmak, K.O. Tozak, A. Mol, A. Mentes, G. Sezen, Extraction and characterization of chitin and chitosan with antimicrobial and antioxidant activities from cosmopolitan Orthoptera species (Insecta), Biotechnol. Bioprocess Eng. 20 (1) (2015) 168–179.
[53] S. Ifuku, R. Nomura, M. Morimoto, H. Saimoto, Preparation of chitin nanofibers from mushrooms, Materials 4 (8) (2011) 1417–1425.
[54] M. Kaya, Y.S. Cakmak, T. Baran, M. Asan-Ozusaglam, A. Mentes, K.O. Tozak, New chitin, chitosan, and *O*-carboxymethyl chitosan sources from resting eggs of Daphnia longispina (Crustacea); with physicochemical characterization, and antimicrobial and antioxidant activities, Biotechnol. Bioprocess. Eng. 19 (1) (2014) 58–69.
[55] M. AbdElhady, Preparation and characterization of chitosan/zinc oxide nanoparticles for imparting antimicrobial and UV protection to cotton fabric, Int. J. Carbohydr. Chem. (2012) 1–6.
[56] L.-H. Li, J.-C. Deng, H.-R. Deng, Z.-L. Liu, L. Xin, Synthesis and characterization of chitosan/ZnO nanoparticle composite membranes, Carbohydr. Res. 345 (8) (2010) 994–998.
[57] V.B. Himes, W.S. Hu, Attachment and growth of mammalian cells on microcarriers with different ion exchange capacities, Biotechnol. Bioeng. 29 (9) (1987) 1155–1163.
[58] K.W. Ng, H.L. Khor, D. Hutmacher, In vitro characterization of natural and synthetic dermal matrices cultured with human dermal fibroblasts, Biomaterials 25 (14) (2004) 2807–2818.
[59] C.S. Ranucci, P.V. Moghe, Substrate microtopography can enhance cell adhesive and migratory responsiveness to matrix ligand density, J. Biomed. Mater. Res. 54 (2) (2001) 149–161.
[60] L. Ponsonnet, V. Comte, A. Othmane, C. Lagneau, M. Charbonnier, M. Lissac, N. Jaffrezic, Effect of surface topography and chemistry on adhesion, orientation and growth of fibroblasts on nickel-titanium substrates, Mater. Sci. Eng.: C. 21 (1) (2002) 157–165.
[61] J. Deutsch, D. Motlagh, B. Russell, T.A. Desai, Fabrication of microtextured membranes for cardiac myocyte attachment and orientation, J. Biomed. Mater. Res. 53 (3) (2000) 267–275.

[62] P. Methacanon, M. Prasitsilp, T. Pothsree, J. Pattaraarchachai, Heterogeneous N-deacetylation of squid chitin in alkaline solution, Carbohydr. Polym. 52 (2) (2003) 119–123.
[63] L.C. Junqueira, J. Carneiro, Basic Histology Text and Atlas, McGraw Hill, London, 2005.
[64] K.S. Kim, J.Y. Lee, Y.M. Kang, E.S. Kim, G.H. Kim, S. Dal Rhee, H.G. Cheon, J.H. Kim, B.-H. Min, H.B. Lee, Small intestine submucosa sponge for in vivo support of tissue-engineered bone formation in the presence of rat bone marrow stem cells, Biomaterials 31 (6) (2010) 1104–1113.
[65] K.S. Kim, J.Y. Lee, Y.M. Kang, E.S. Kim, B. Lee, H.J. Chun, J.H. Kim, B.H. Min, H.B. Lee, M.S. Kim, Electrostatic crosslinked in Situ–forming in vivo scaffold for rat bone marrow mesenchymal stem cells, Tissue Eng. A 15 (10) (2009) 3201–3209.
[66] H.H. Ahn, K.S. Kim, J.H. Lee, J.Y. Lee, B.S. Kim, I.W. Lee, H.J. Chun, J.H. Kim, H.B. Lee, M.S. Kim, In vivo osteogenic differentiation of human adipose-derived stem cells in an injectable in situ–forming gel scaffold, Tissue Eng. A 15 (7) (2009) 1821–1832.
[67] S. Leibovich, Promotion of wound repair in mice by application of glucan, J. Reticuloendothel. Soc. 27 (1980) 1–11.
[68] W. Browder, D. Williams, P. Lucore, H. Pretus, E. Jones, R. McNamee, Effect of enhanced macrophage function on early wound healing, Surgery 104 (2) (1988) 224–230.
[69] H. Ueno, H. Yamada, I. Tanaka, N. Kaba, M. Matsuura, M. Okumura, T. Kadosawa, T. Fujinaga, Accelerating effects of chitosan for healing at early phase of experimental open wound in dogs, Biomaterials 20 (15) (1999) 1407–1414.
[70] K. Azuma, R. Izumi, T. Osaki, S. Ifuku, M. Morimoto, H. Saimoto, S. Minami, Y. Okamoto, Chitin, chitosan, and its derivatives for wound healing: old and new materials, J. Funct. Biomater. 6 (1) (2015) 104–142.
[71] R.A. Muzzarelli, Chitins and chitosans for the repair of wounded skin, nerve, cartilage and bone, Carbohydr. Polym. 76 (2) (2009) 167–182.
[72] P. Brychta, J. Adler, H. Řihová, I. Suchánek, Y. Kaloudová, J. Koupil, Cultured epidermal allografts: quantitative evaluation of their healing effect in deep dermal burns, Cell Tissue Bank. 3 (1) (2002) 15–23.
[73] Z. Wu, Y. Ding, L. Zhang, S. Zhong, T. Jiang, Primary grafting research of tissue engineered oral mucosa lamina propria on skin full thickness wounds, Chin. J. Repara. Recons. Surg. 20 (2) (2006) 172–176.
[74] H.B. Tvl, M. Vidyavathi, K. Kavitha, T. Sastry, S.K. RV, Preparation and evaluation of ciprofloxacin loaded chitosan-gelatin composite films for wound healing activity, Int. J. Drug Deliv. 2 (2) (2010).